ADVANCED OPTICAL MATERIALS
www.advopticalmat.de

Selective Out-of-Plane Optical Coupling between Vertical and Planar Microrings in a 3D Configuration

Sreeramulu Valligatla, Jiawei Wang, Abbas Madani, Ehsan Saei Ghareh Naz, Qi Hao, Christian Niclaas Saggau, Yin Yin, Libo Ma,* and Oliver G. Schmidt*

3D photonic integrated circuits are expected to play a key role in future optoelectronics with efficient signal transfer between photonic layers. Here, the optical coupling of tubular microcavities, supporting resonances in a vertical plane, with planar microrings, accommodating in-plane resonances, is explored. In such a 3D coupled composite system with largely mismatched cavity sizes, periodic mode splitting and resonant mode shifts are observed due to mode-selective interactions. The axial direction of the microtube cavity provides additional design freedom for selective mode coupling, which is achieved by carefully adjusting the axial displacement between the microtube and the microring. The spectral anticrossing behavior is caused by strong coupling in this composite optical system and is excellently reproduced by numerical modeling. Interfacing tubular microcavities with planar microrings is a promising approach toward interlayer light transfer with added optical functionality in 3D photonic systems.

1. Introduction

3D photonic integrated circuits (PICs) are key to overcome intrinsic limitations in 2D PICs and push optical systems toward low-power consumption and high-density functionalities in a 3D integrated photonic chip.[1–3] In conventional 2D PICs, where all devices reside in the same plane, microring resonators are the main building blocks for various on-chip photonic and optoelectronic systems,[4] serving as optical filters,[5] modulators,[6] and frequency comb generators,[7] to name a few. Furthermore, micro/nanoresonator coupling in one plane has been widely investigated[8–13] for applications such as wavelength division multiplexing,[14] sensing,[15] and lasing modulation.[16] In recent years, various schemes have been proposed to conquer the third dimension, such as laser inscription of 3D waveguide circuits,[17] interlayer grating couplers for vertical integration of multiple photonic components,[18–20] and photonic routing architectures based on multiple waveguides for out-of-plane light coupling.[21] However, these schemes mainly rely on simple passive light transfer components, which do not use the 3D space efficiently. For high-density 3D photonic integration, a new approach is required to not only transfer light from layer to layer but also to fill the space in between the layers with photonic functionalities such as flexible reorientation of light propagation and wavelength-selective transfer between different layers.

In contrast to planar ring resonators, a microtube optical ring resonator is able to support out-of-plane whispering gallery modes (WGM) in the vertical direction,[22,23] therefore providing a concept to also exploit the vertical direction with additional

Dr. S. Valligatla, Dr. J. Wang, Dr. A. Madani, E. S. G. Naz, Dr. Q. Hao, C. N. Saggau, Dr. Y. Yin, Dr. L. Ma, Prof. O. G. Schmidt
Institute for Integrative Nanosciences
IFW Dresden
Helmholtzstr. 20, Dresden 01069, Germany
E-mail: jiawei.wang@ifw-dresden.de; l.ma@ifw-dresden.de

Dr. J. Wang, Prof. O. G. Schmidt
Material Systems for Nanoelectronics
Technische Universität Chemnitz
Reichenhainer Str. 70, Chemnitz 09107, Germany

Dr. J. Wang
Department of Electronic and Information Engineering
Harbin Institute of Technology (Shenzhen)
Shenzhen 518055, China

The ORCID identification number(s) for the author(s) of this article can be found under https://doi.org/10.1002/adom.202000782.

DOI: 10.1002/adom.202000782

Dr. A. Madani
Department of Engineering
The University of Cambridge
9 JJ Thomson Avenue, Cambridge CB3 OFA, UK

Dr. Q. Hao
School of Physics
Southeast University
Nanjing 211189, China

Prof. O. G. Schmidt
Research Center for Materials, Architectures and Integration of Nanomembranes (MAIN)
Technische Universität Chemnitz
Rosenbergstrasse 6, Chemnitz 09126, Germany

Prof. O. G. Schmidt
Nanophysics
Faculty of Physics
TU Dresden
Dresden 01062, Germany

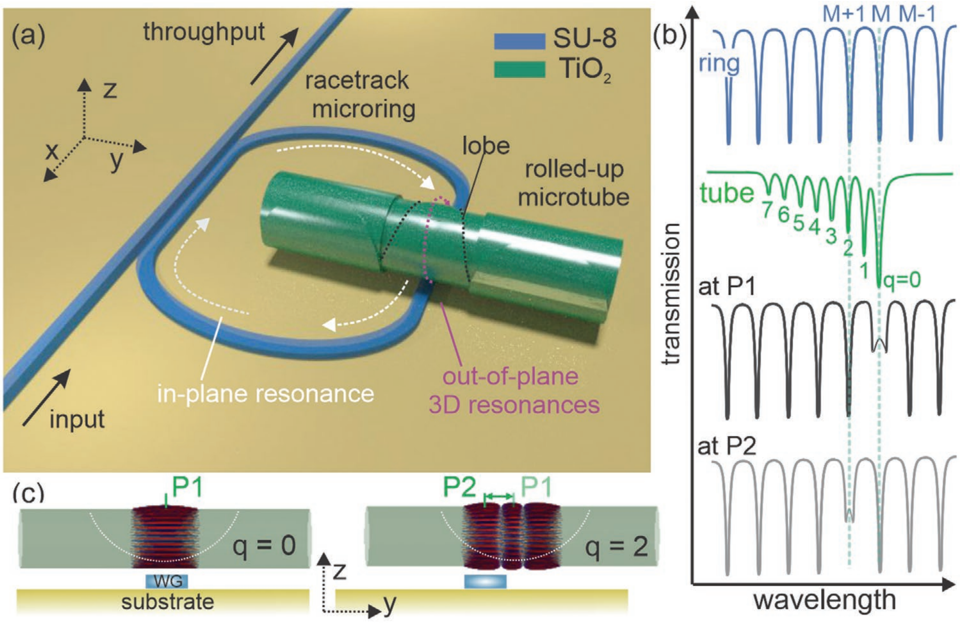

Figure 1. a) Schematic of a coupled composite cavity system compromising a microtube and a planar racetrack microring. The resonant trajectories are labeled by white dashed arrow lines (planar resonances) and purple dashed arrow lines (vertical resonances), respectively. b) Schematic of the transmission spectra of planar racetrack microring (blue), axial resonance modes in the microtube cavity (green), and the microtube cavity coupled to planar racetrack microring at P1 (black) and P2 (gray) sites, respectively. c) Sketch of view in the y–z plane for microtube cavity integrated with an on-chip waveguide with fundamental and axial modes at coupling site P1 (lobe center aligned with the waveguide core, left panel) and slightly shifted position P2 (lobe center slightly misaligned with the waveguide core, right panel), respectively.

functionality such as opto-plasmonic coupling,[24] out-of-plane directional control of light emission,[25] microcavity-based spin–orbit coupling,[26] or even optofluidic detection in lab-in-a-tube systems.[27] Intriguingly, such vertical ring resonators are compatible with on-chip monolithic integration if manufactured by rolled-up nanotechnology.[28–37] As a first key step toward efficient 3D photonic integration, we therefore design and investigate the coupling of a rolled-up tubular microcavity positioned on a planar microring structure. We demonstrate axial-dependent selective mode coupling between out-of-plane resonant modes supported by the microtube cavity and in-plane resonances of the planar microring. Strong optical coupling is revealed by a mode splitting larger than the mode linewidth and a pronounced anticrossing behavior upon spectral detuning.

2. Results and Discussions

2.1. Working Principle

Figure 1a shows the schematic of the microtube cavity coupled to a planar microring. The racetrack-shaped planar microring resonator is evanescently coupled to a bus waveguide carrying the input and throughput coupling signals. Similar to previous reports, a lobe structure was designed in the middle of the microtube providing axial mode confinement.[38,39] Although the resonant orbits in the microtube cavity and the planar ring resonator propagate in two orthogonal planes, their coupling is allowed due to the wave vector match at their contacting point. Figure 1b shows a schematic illustration of the resonant spectra of the planar ring, microtube cavity, and the coupled cavity system, respectively.

Because of the distinct spatial distribution of the optical axial modes in the microtube cavity, resonant modes in the planar ring can be selectively coupled to different order axial modes in the tube cavity depending on the coupling position (e.g., P1 and P2 in Figure 1c). For instance, when the lobe center (P1) is aligned to the core of the planar ring segment, the fundamental mode (denoted as $q = 0$) of the microtube cavity is coupled to the planar ring owing to the spatially overlapping resonant mode fields. As such, efficient energy transfer and strong coupling occurs with a remarkable mode splitting. The coupling effect changes significantly even for a small displacement (≈7 µm) of the tube position to P2. At P2, the resonance mode in the microring mostly overlaps with the second-order axial mode. Because the FSR of the higher-order axial modes is comparable to that of the azimuthal modes in the planar ring, the fundamental and higher-order axial modes can couple to the ring modes with different azimuthal mode numbers, e.g., M and M+1, respectively. Thus, the efficient intercavity coupling can be tuned and determined by carefully adjusting and positioning the microtube cavity on the planar ring. In the present work, we demonstrate coupling at P1 and P2, which is sufficient to claim tunable and selective coupling in this novel 3D microcavity system.

2.2. Fabrication and Characterizations

On-chip SU-8 polymer (refractive index $n \approx 1.57$@1550 nm) based waveguides and racetrack microrings were fabricated using electron-beam lithography (see the Experimental Section). TiO_2 with a transparency window from visible to near-

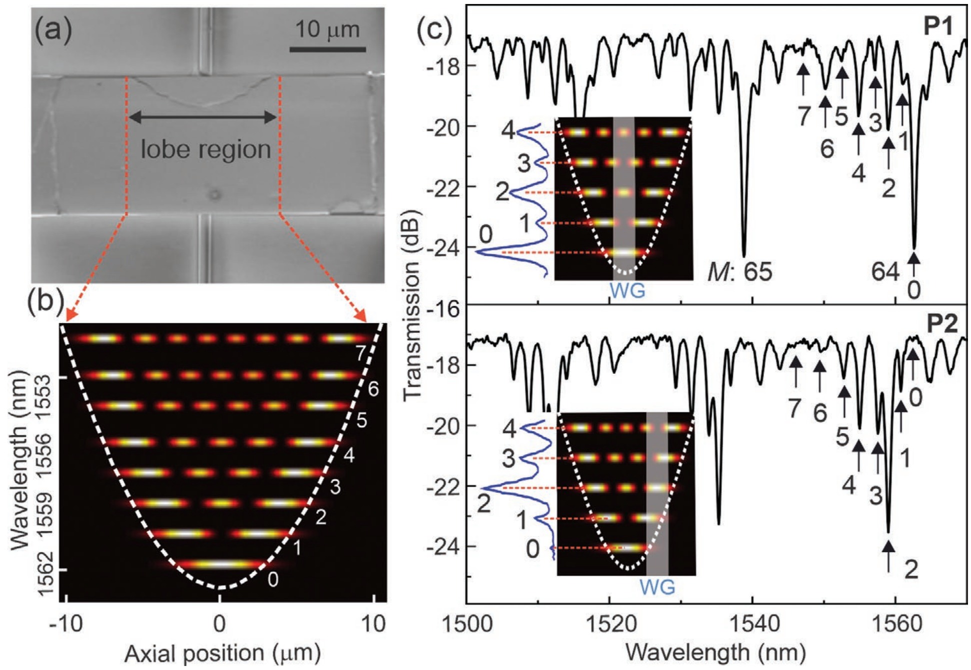

Figure 2. a) Top-view SEM image of a TiO_2 microtube cavity coupled to an on-chip SU-8 waveguide. The dotted line represents the lobe region. b) Calculated mode field intensity distributions of axial modes ($q = 0$–7) for azimuthal mode $M = 64$. c) Transmission spectra of TiO_2 microtube cavity coupled to SU-8 waveguide (WG), measured at the center (P1) and edge side (P2) of the lobe. Axial modes are discerned as $q = 0$–7 for the azimuthal mode $M = 64$. Insets: Mode field intensity distributions (for $q = 0$–4) together with corresponding resonant spectra coupled with WG at P1 and P2. The gray shaded areas represent the waveguide locations.

infrared wavelengths is chosen due to its high refractive index ($n \approx 2.40$@1550 nm) for efficient optical confinement in thin-walled tubular microcavities. The microtube cavities were fabricated by rolling up prestrained TiO_2 nanomembranes from a U-shape pattern with a lobe structure designed in the middle position, followed by 50 nm TiO_2 coating via atomic layer deposition. The roll-up of a 75 nm thick TiO_2 nanomembrane for ≈2.1 windings results in a cavity wall thickness of ≈250 nm. Optical characterization at telecom wavelengths was conducted by a butt-coupling setup (see the Experimental Section).

A scanning electron microscopy (SEM) image of a microtube cavity with a diameter of ≈15.9 µm coupled to an SU-8 waveguide is shown in **Figure 2**a. TiO_2 microtubes were transferred onto SU-8 waveguides and/or microrings using a micromanipulator. The direct contact between the microtube and the waveguide or planar microring ensures efficient light coupling between the resonant modes in the vertical microring cavity and the waveguide mode in the planar devices. Mode field distributions of axial modes (labeled as $q = 0$–7) for azimuthal mode $M = 64$ are calculated by solving the eigenstates in an optical quasi-potential well[39,40] (see Figure 2b). Figure 2c shows the transmission spectra of the TiO_2 microtube cavity coupled to an SU-8 waveguide measured at P1 and P2, respectively. Optical microscopy images of the TiO_2 microtube cavity coupled to the on-chip SU-8 waveguide at P1 and P2 are shown in Figure S2 (Supporting Information). In our configuration, the SU-8-based devices are fixed on the substrate while the axial modes in the microtube can be "selected" by shifting the microtube along the axial direction, for instance, from P1 to P2 (see Figure S2, Supporting Information).

Because of the ultrathin tube wall, only transverse-magnetic (TM) modes (electric field parallel to the tube axis) are supported and labeled by $M = 64$–66 in the transmission spectra. At P1, three sets of azimuthal modes ($M = 64$–66) supported by the microtube cavity are displayed in the transmission spectrum. Along with the fundamental mode ($q = 0$), higher-order axial modes represented by $q = 1$–7 are also observed at each azimuthal mode. Due to the designed parabolic lobe shape, higher-order axial modes with the same azimuthal mode number are nearly equally separated with a spacing of ≈3.5 nm, which agrees well with the calculation results in Figure 2b (see Figure S4, Supporting Information). The spectrum of the coupled system at P2 was measured after moving the tube ≈7 µm along its axial direction, as shown in Figure 2c. Instead of the fundamental mode, the higher-order modes ($q = 2$) are selectively excited because of the overlapping of their mode fields. The measured extinction ratio strongly depends on the spatial overlapping between the waveguide and the antinodes of each axial mode in the tubular microcavity. At P1, the waveguide largely overlaps with higher-order modes $q = 0, 2, 4$ which results in an alternating variation of the corresponding resonant dips. At P2, the waveguide mainly overlaps with higher-order modes $q = 2$, 4 and less with modes $q = 0, 1, 3$.

Figure 3a shows top-view optical microscopy images of SU-8 planar racetrack microrings coupled to the TiO_2 microtube cavity at P1 and P2 positions. The transmission spectrum of an individual planar microring in the upper panel of Figure 3b shows periodic transmission dips (labeled by $M = 434$–451) with an FSR of ≈3.59 nm, which is ≈7 times smaller than that

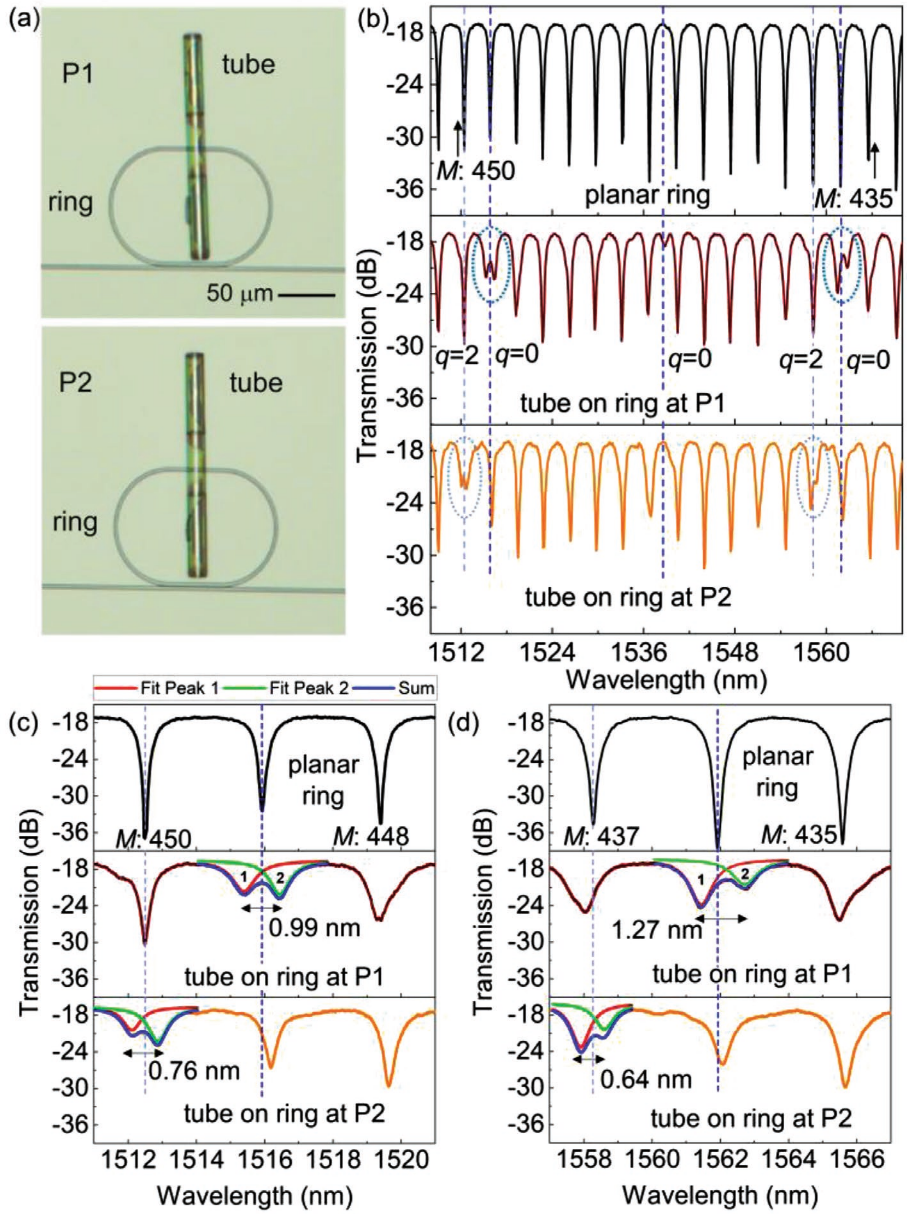

Figure 3. a) Optical microscopy images of TiO_2 microtube cavity coupled to SU-8 planar racetrack microring at P1 and P2. The width and height of the waveguide are 3 and 1.8 μm, respectively. The radius of the ring is 50 μm, the interaction length is 50 μm, and the gap between the ring and the straight waveguide is 750 nm. b) Transmission spectra of planar racetrack microring (upper panel), microtube cavity coupled to planar microring at the center of the lobe at P1 (middle panel) and end of the lobe at P2 (lower panel). The dashed line indicates fundamental ($q = 0$) and higher-order ($q = 2$) modes of microtube cavity coupling with resonances of the planar ring. c,d) Transmission spectra of microring (black), coupled system measured at P1 (wine) and at P2 (orange) in the range of 1511–1521 and 1557–1567 nm, respectively.

of the microtube. At coupling position P1 (e.g., the center of the lobe), the fundamental mode of the TiO_2 microtube cavity and the mode of the planar racetrack microring is spectrally matched at 1515.8 nm and nearly matched at 1561.9 nm, hence allowing efficient light interaction, as shown in the middle panel of Figure 3b. After changing the relative displacement between the ring and tube by moving the tube ≈7 μm along the axial direction (at P2), the fixed ring modes interact with higher-order axial modes ($q = 2$) at 1512.4 and 1558.3 nm, which results in a mode splitting as shown in the lower panel of Figure 3b. At coupling position P1, the fundamental mode of the microtube at 1538.7 nm is completely mismatched with the resonant ring modes, and only a minor dip appears in the coupled cavity resonant spectrum in the middle panel of Figure 3b.

Figure 3c,d takes a close look of Figure 3b in the range from 1511 to 1521 and 1557 to 1567 nm, revealing clear mode splitting features for the modes $M = 436$, 437, 449, and 450. The modifications in the coupled cavity system can be quantitatively analyzed by fitting the resonant modes with multiple Lorentzian lines and extracting the linewidths and mode shifts. The spectral shift is defined as the wavelength offset between the original resonant mode and the principal one (with the larger extinction ratio) out of the two split modes. Different splittings are extracted for the fundamental (0.99 and 1.27 nm) and second-order axial mode (0.76 and 0.64 nm). The splittings in the coupled cavity are larger than the average linewidths of the microtube cavity and planar microring, hence satisfies the strong coupling criterion.[41] A mode shift of ≈0.5 and ≈0.3 nm is observed for the planar ring after coupling with the fundamental and higher-order modes of the microtube cavity, respectively. Because the coupling strength (proportional to the field overlapping with the waveguide to the whole respective mode field) decreases for the higher-order axial mode, the mode shift of the fundamental mode is larger than that of the higher-order axial mode. Additional measurements on rolled-up microtube with lobe design coupled to the planar microring with different device parameters reveal consistent phenomena (see Section S3, Supporting Information).

Furthermore, the coupling behavior of the rolled-up microtube without the lobe design coupled to the planar microring was characterized as a control experiment (see Section S4, Supporting Information). Compared to the coupled system with the lobe design, the resonances along the tubular cavity without the lobe-induced axial confinement suggest a larger mode volume, and hence a decreased mode overlapping (effectively the coupling strength) with the ring mode.

2.3. Numerical Simulations

The coupling behavior of two size-mismatched cavities can be studied using transfer matrix modeling (see Section S5, Supporting Information). The input and cross-coupling coefficients are extracted by fitting the measurement results in Figures 2 and 3. The cross-coupling coefficient for the strong coupling case at P1 in **Figure 4**a is extracted as ≈0.38. For the case at P2, it drops to ≈0.30. Figure 4a presents the modeled transmission spectra for an individual microring and the integrated system reproducing the different coupling strength at P1 and P2. The fundamental and higher-order modes of the microtube cavity located at 1514.78 and 1511.20 nm are spectrally aligned with the resonant modes of the microring, which leads to selective mode splitting. The zoomed-in view in Figure 4b reveals clear splitting widths of 1.00 and 0.72 nm for the fundamental and higher-order axial mode coupling to the planar ring resonant modes (M = 449 and 450), respectively. Figure 4c reveals a mode shift of 0.7 nm for the hybridized mode between the ring mode and originally the fundamental tube mode while the shift decreases to 0.4 nm for the hybridized mode between ring mode and originally the second-order tube axial mode. In Figure 4d, the Q factor of the coupled system remains almost unperturbed for modes with inefficient coupling, suggesting minor perturbation by tube-induced scattering. The reduction of the Q factor (≈2300–2600) for coupled modes with efficient coupling is due to the mixing and energy transfer between the ring mode and the tube mode.

2.4. Anticrossing Behavior of Coupled Modes

The strong coupling between the planar ring and microtube cavity is further verified by thermo-optic tuning of the resonances. In the calibration tests of individual cavities, the SU-8 planar microring experiences a spectral blueshift upon heating at a rate of ≈0.137 nm $°C^{-1}$ due to the large negative thermo-optic coefficient[42] (see Section S6, Supporting Information). For the TiO_2 microtube cavity, a minor spectral blueshift upon heating at a rate of ≈0.045 nm $°C^{-1}$ is mainly attributed to inefficient heat transfer to the microtube and a small thermo-optic coefficient of TiO_2[43] (see the Supporting Information). While the ring modes with inefficient coupling reveal a total shift of ≈3.3 nm upon heating from room temperature (24 °C) to 48 °C, the dominating mode of the split modes (around 1538 nm) with a large extinction ratio gradually changes from the long-wavelength branch to the short-wavelength branch (see **Figure 5**a). This is due to the spectral detuning of the original ring mode across the tube mode in the coupled split mode. As presented in Figure 5b, the mode splitting first shrinks from 1.48 to 1.06 nm, and increases back to 1.86 nm upon thermal tuning, which agrees with the anticrossing feature observed in conventional dual-element microresonators.[44,45]

The strong coupling behavior in the coupled cavity is modeled using the transfer-matrix method. Figure 5c shows the modeled transmission spectra obtained by varying n_{eff} of the system, which mimics the temperature change. The resonant modes of the ring and tube are blueshifted with 3.4 and 1.1 nm, respectively, with corresponding changes in their n_{eff} (−0.0045 for the ring and −0.0015 for the tube). Figure 5d shows that the split modes with a spacing of 1.6 nm approach each other as n_{eff} increases, the splitting reaches a minimum of 1.1 nm and then gradually separates again. The anticrossing feature agrees well with our experimental results.

3. Conclusion and Outlook

In conclusion, out-of-plane resonant coupling is enabled by combining a microtube cavity and a planar microring cavity in a 3D configuration. The fundamental and higher-order axial modes confined in the tubular microcavity are selectively coupled with resonance modes of the planar racetrack microring resonator by adjusting the coupling site along the tube axial direction on the planar microring. Clear spectral anticrossing behavior is observed as direct evidence of strong coupling in the cavity composite. Theoretical modeling results agree well with experimental results.

For future 3D PICs, this work offers a potential route to efficiently utilize space between photonic layers for light transfer. Based on mature monolithic integration technologies,[22,34–37] accurately oriented tubular cavity will lead to flexibly engineered out-of-plane resonant orbits and possibilities for light coupling into different directions in an upper waveguiding layer. The direct self-rolling on top of the as-fabricated microrings can be implemented by patterning a strained nanomembrane on a sacrificial layer spin-coated on the planar ring. This strategy

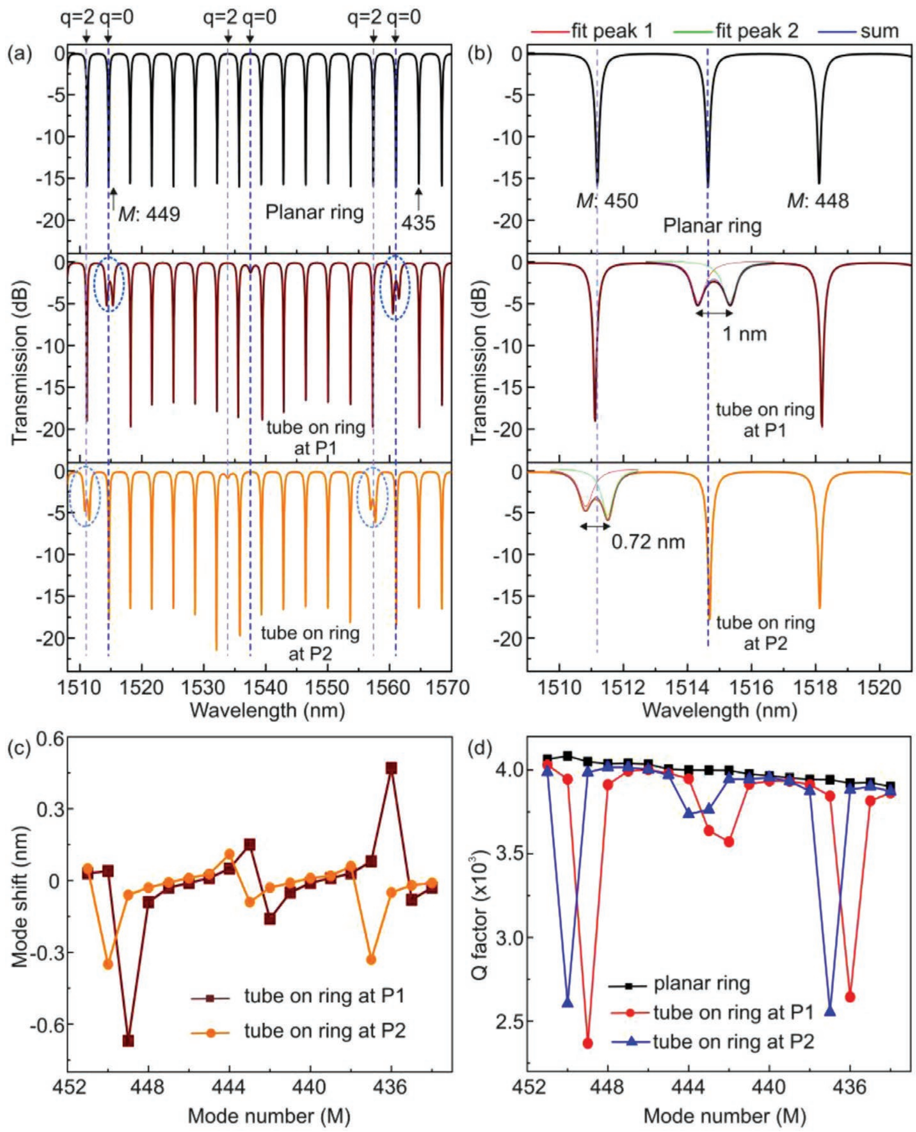

Figure 4. a) Modeled resonant spectra of the planar racetrack microring (upper) and microtube cavity coupled to planar racetrack microring at P1 (middle) and P2 (lower). The dashed line indicates fundamental ($q = 0$) and higher-order ($q = 2$) modes of microtube cavity coupled with resonances of the planar ring. b) Transmission spectra in in the range of 1509–1521 nm. c) Mode shift as a function of the mode number for the coupled system at P1 and P2 and d) Q factor as a function of the mode number for the coupled system at P1 and P2 and the individual microring.

would allow precise and flexible control of the tube orientation and coupling position through lithography (see Section S7, Supporting Information). Besides, the coupling gap spacing can also be adjusted by changing the thickness of the photoresist and the rounds of self-rolling. As such, changing from the current gapless coupling to variable gap spacing will provide a new control knob to adjust the coupling strength. Besides, owing to the additional degree of freedom along the axial direction, the densely spaced yet controllable axial modes will be promising as multiplexed channels in future on-chip optical switches or sensors.

4. Experimental Section

Fabrication of TiO_2 Rolled-Up Microtube Cavities and SU-8 Devices: TiO_2 rolled-up microcavities were fabricated by rolling up prestrained TiO_2 nanomembranes from a U-shape pattern with lobe structure designed in the middle position.[34,38] In brief, 1.5 µm thick photoresist (AR-P 3510, Allresist GmbH) as a sacrificial layer, was first patterned on a silicon substrate coated with 1.5 µm thick thermally grown oxide layer by a maskless lithography process (μPG 101, Heidelberg Instruments). Afterward, a differentially strained TiO_2 nanomembrane (75 nm thick) was deposited by evaporating Ti metal in an oxygen atmosphere using angled electron-beam evaporation (Edwards Auto500 e-beam) at a glancing angle of 15°. The difference of TiO_2 deposition rates from 0.3 Å s^{-1} (15 nm) to 3 Å s^{-1} (60 nm) leads to differentially strained layers for rolling. The rolling occurred when the photoresist was dissolved in an organic solvent (dimethyl sulfoxides, DMSO). A critical point dryer (931 GL, Tousimis CPD) was employed to avoid the structure changes during the evaporation of solvents. At last, a 50 nm thick TiO_2 film was coated on the microtube cavity surface using atomic layer deposition (FlexAL, Oxford Instruments PLC, Abingdon, UK) to increase the structural stability and the optical confinement. The empirical studies

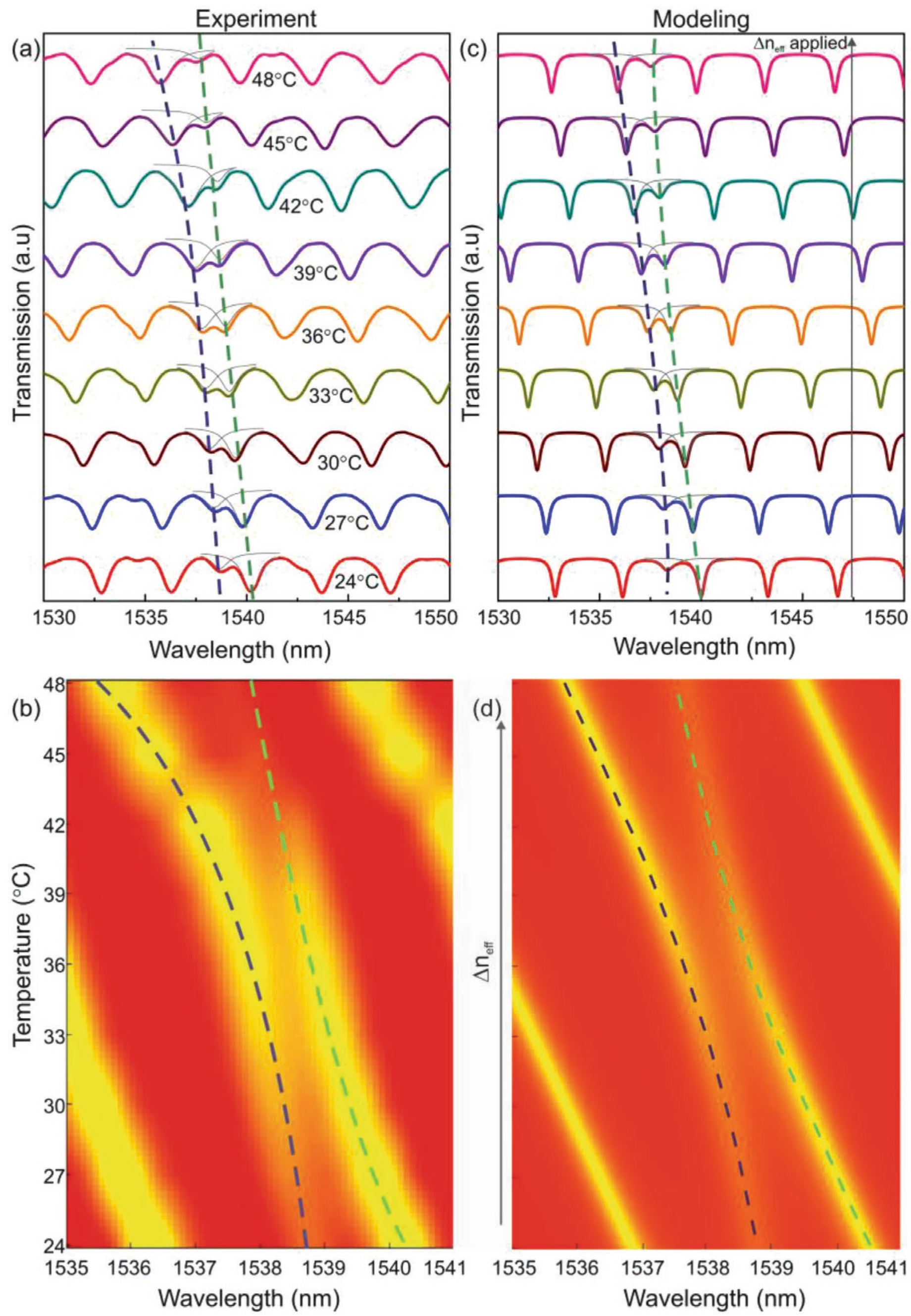

Figure 5. a) Transmission spectra of the coupled cavity system measured by varying the substrate temperature. The gray lines indicate the two Lorentzian fits for the split modes. b) Evolution of the fitted split modes showing clear anticrossing behavior. The dashed lines serve as visual aids for tracing the split mode wavelengths. c) Modeled transmission spectra of the coupled cavity system obtained by varying n_{eff} of two cavities. d) Evolution of the modeled split modes.

suggest that tubes with a diameter ≈10–20 µm and winding numbers ≈2–3 show optimal yields. Through atomic layer deposition to further increase the tube wall thickness optical resonances at ≈1550 nm are well supported and the FSR can be tuned over a range of 2–5 nm.

SU-8 polymer (MicroChem) based waveguide coupled planar racetrack microring resonators were fabricated on silicon substrates (coated with 3.1 µm thick oxide layer) using electron beam lithography (Raith EBL Voyager) and wet etching development from a 1.8 µm thick SU-8 layer following the standard fabrication process.[46]

Optical Characterization by Butt-Coupling Setup: Optical characterization was carried out using butt-coupling experiment, shown in Figure S3 (Supporting Information). A wavelength-tunable infrared laser (1440–1640 nm, Yenista, Tunics 100S-HP) was used as a light source. The laser light was launched into a tapered on-chip SU-8 waveguide through a single-mode lensed fiber (Chuxing Fiber). The polarization state of the input light was controlled by a fiber-based polarization controller. The output signal was collected by a multimode lensed fiber which was connected to an InGaAs photodetector-based IR detection system. The chip under the thermal-tuning test was mounted on a thermoelectric cooler (TEC). The local temperature was monitored by a temperature transducer (AD 590) and a controller (TED200C, Thorlabs). The total insertion loss of the coupled system is ≈17 dB. The majority of the loss is attributed to the coupling loss between the waveguide facet and the lensed fiber at both the input and output side (>5 dB for each).

Supporting Information

Supporting Information is available from the Wiley Online Library or from the author.

Acknowledgements

The authors acknowledge financial support from the DFG (Leibniz Program and SCHM 1298/22-1 and FO 956/4-1) through the Würzburg-Dresden Cluster of Excellence on Complexity and Topology in Quantum Matter – ct.qmat (EXC 2147, project-id 390858490). O.G.S. acknowledges financial support by the Leibniz Program of the German Research Foundation (SCHM 1298/26-1). The authors thank Engelhard Ronny and Martin Bauer for the technical support in the cleanroom.

Open access funding enabled and organized by Projekt DEAL.

Conflict of Interest

The authors declare no conflict of interest.

Keywords

3D photonic integration, out-of-plane coupling, planar microrings, strong coupling, tubular microcavities

Received: May 12, 2020
Revised: August 4, 2020
Published online:

[1] N. Nishiyama, J. Kang, Y. Kuno, K. Itoh, Y. Atsumi, T. Amemiya, S. Arai, *IEICE Trans. Electron.* **2018**, *E101.C*, 501.
[2] T. Tajiri, S. Takahashi, Y. Ota, K. Watanabe, S. Iwamoto, Y. Arakawa, *Optica* **2019**, *6*, 296.
[3] Y. Zhang, Y. Ling, Y. Zhang, K. Shang, S. J. B. Yoo, *IEEE J. Sel. Top. Quantum Electron.* **2018**, *24*, 8200510.
[4] Z. Yao, K. Wu, B. X. Tan, J. Wang, Y. Li, Y. Zhang, A. W. Poon, *IEEE J. Sel. Top. Quantum Electron.* **2018**, *24*, 1.
[5] J. Niehusmann, A. Vörckel, P. H. Bolivar, T. Wahlbrink, W. Henschel, H. Kurz, *Opt. Lett.* **2004**, *29*, 2861.
[6] Q. Xu, B. Schmidt, S. Pradhan, M. Lipson, *Nature* **2005**, *435*, 325.
[7] A. L. Gaeta, M. Lipson, T. J. Kippenberg, *Nat. Photonics* **2019**, *13*, 158.
[8] S. V. Boriskina, *Opt. Lett.* **2007**, *32*, 1557.
[9] B. Peng, Ş. K. Özdemir, J. Zhu, L. Yang, *Opt. Lett.* **2012**, *37*, 3435.
[10] T. Grossmann, T. Wienhold, U. Bog, T. Beck, C. Friedmann, H. Kalt, T. Mappes, *Light: Sci. Appl.* **2013**, *2*, e82.
[11] C. Yang, X. Jiang, Q. Hua, S. Hua, Y. Chen, J. Ma, M. Xiao, *Laser Photonics Rev.* **2017**, *11*, 1600178.
[12] Y. Li, F. Abolmaali, K. W. Allen, N. I. Limberopoulos, A. Urbas, Y. Rakovich, A. V. Maslov, V. N. Astratov, *Laser Photonics Rev.* **2017**, *11*, 1600278.
[13] T. Siegle, S. Schierle, S. Kraemmer, B. Richter, S. F. Wondimu, P. Schuch, C. Koos, H. Kalt, *Light: Sci. Appl.* **2017**, *6*, e16224.
[14] D. Dai, *J. Lightwave Technol.* **2017**, *35*, 572.
[15] J. Wang, Z. Yao, T. Lei, A. W. Poon, *Sci. Rep.* **2015**, *4*, 7528.
[16] S. Ishii, T. Baba, *Appl. Phys. Lett.* **2005**, *87*, 181102.
[17] S. J. B. Yoo, B. Guan, R. P. Scott, *Microsyst. Nanoeng.* **2016**, *2*, 16030.
[18] K. Shang, S. Pathak, B. Guan, G. Liu, S. J. B. Yoo, *Opt. Express* **2015**, *23*, 21334.
[19] M. Sodagar, R. Pourabolghasem, A. A. Eftekhar, A. Adibi, *Opt. Express* **2014**, *22*, 16767.
[20] R. Takei, Y. Maegami, E. Omoda, Y. Sakakibara, M. Mori, T. Kamei, *Opt. Express* **2015**, *23*, 18602.
[21] J. Chiles, S. Buckley, N. Nader, S. W. Nam, R. P. Mirin, J. M. Shainline, *APL Photonics* **2017**, *2*, 116101.
[22] X. Li, *Adv. Opt. Photonics* **2011**, *3*, 366.
[23] C. Strelow, C. M. Schultz, H. Rehberg, M. Sauer, H. Welsch, A. Stemmann, C. Heyn, D. Heitmann, T. Kipp, *Phys. Rev. B* **2012**, *85*, 155329.
[24] Y. Yin, J. Pang, J. Wang, X. Lu, Q. Hao, E. S. G. Naz, X. Zhou, L. Ma, O. G. Schmidt, *ACS Appl. Mater. Interfaces* **2019**, *11*, 15891.
[25] J. Wang, Y. Yin, Y.-D. Yang, Q. Hao, M. Tang, X. Wang, C. N. Saggau, D. Karnaushenko, X. Yan, Y.-Z. Huang, L. Ma, O. G. Schmidt, *ACS Photonics* **2019**, *6*, 2537.
[26] L. B. Ma, S. L. Li, V. M. Fomin, M. Hentschel, J. B. Götte, Y. Yin, M. R. Jorgensen, O. G. Schmidt, *Nat. Commun.* **2016**, *7*, 10983.
[27] S. M. Harazim, V. A. B. Quiñones, S. Kiravittaya, S. Sanchez, O. G. Schmidt, *Lab Chip* **2012**, *12*, 2649.
[28] F. Li, Z. Mi, *Opt. Express* **2009**, *17*, 19933.
[29] Z. Tian, V. Veerasubramanian, P. Bianucci, S. Mukherjee, Z. Mi, A. G. Kirk, D. V. Plant, *Opt. Express* **2011**, *19*, 12164.
[30] P. Bianucci, S. Mukherjee, M. H. T. Dastjerdi, P. J. Poole, Z. Mi, *Appl. Phys. Lett.* **2012**, *101*, 031104.
[31] Q. Zhong, Z. Tian, M. H. T. Dastjerdi, Z. Mi, D. V. Plant, *Opt. Express* **2013**, *21*, 18909.
[32] S. Böttner, S. L. Li, M. R. Jorgensen, O. G. Schmidt, *Appl. Phys. Lett.* **2013**, *102*, 251119.
[33] X. Yu, L. L. Goddard, X. Li, X. Chen, *Appl. Phys. Lett.* **2016**, *109*, 111104.
[34] A. Madani, M. Kleinert, D. Stolarek, L. Zimmermann, L. Ma, O. G. Schmidt, *Opt. Lett.* **2015**, *40*, 3826.
[35] X. Yu, E. Arbabi, L. L. Goddard, X. Li, X. Chen, *Appl. Phys. Lett.* **2015**, *107*, 031102.
[36] A. Madani, S. M. Harazim, V. A. B. Quiñones, M. Kleinert, A. Finn, E. S. G. Naz, L. Ma, O. G. Schmidt, *Opt. Lett.* **2017**, *42*, 486.
[37] X. Yu, L. L. Goddard, J. Zhu, X. Li, X. Chen, *Appl. Phys. Lett.* **2018**, *112*, 021108.
[38] C. Strelow, H. Rehberg, C. M. Schultz, H. Welsch, C. Heyn, D. Heitmann, T. Kipp, *Phys. Rev. Lett.* **2008**, *101*, 127403.
[39] Y. Yin, S. Li, S. Böttner, F. Yuan, S. Giudicatti, E. S. G. Naz, L. Ma, O. G. Schmidt, *Phys. Rev. Lett.* **2016**, *116*, 253904.
[40] J. Wang, Y. Yin, Q. Hao, S. Huang, E. S. G. Naz, O. G. Schmidt, L. Ma, *ACS Photonics* **2018**, *5*, 2060.
[41] P. Törmä, W. L. Barnes, *Rep. Prog. Phys.* **2015**, *78*, 013901.
[42] Y. Zhang, P. Liu, S. Zhang, W. Liu, J. Chen, Y. Shi, *Opt. Express* **2016**, *24*, 23037.
[43] O. Reshef, K. Shtyrkova, M. G. Moebius, S. Griesse-Nascimento, S. Spector, C. C. Evans, E. Ippen, E. Mazur, *J. Opt. Soc. Am. B* **2015**, *32*, 2288.
[44] M. Benyoucef, S. Kiravittaya, Y. F. Mei, A. Rastelli, O. G. Schmidt, *Phys. Rev. B* **2008**, *77*, 035108.
[45] B. S. Lee, M. Zhang, F. A. S. Barbosa, S. A. Miller, A. Mohanty, R. St-Gelais, M. Lipson, *Opt. Express* **2017**, *25*, 12109.
[46] D. Dai, B. Yang, L. Yang, Z. Sheng, *Proc. SPIE* **2008**, *7134*, 713414.